Cathodoluminescence and Trace Elements in Quartz: Clues to Metal Precipitation Mechanisms at the Asachinskoe Gold Deposit in Kamchatka

Ryohei Takahashi[1,*], Axel Müller[2], Hiroharu Matsueda[3], Victor M. Okrugin[4], Shuji Ono[5], Alfons van den Kerkhof[6], Andreas Kronz[6] and Elena D. Andreeva[4]

[1]*COE for Neo-Science of Natural History, Graduate School of Science, Hokkaido University, Sapporo, Japan*
[2]*Geological Survey of Norway, Trondheim, Norway*
[3]*The Hokkaido University Museum, Sapporo, Japan*
[4]*Institute of Volcanology and Seismology, Far Eastern Division, Russian Academy of Science, Petropavlovsk-Kamchatsky, Russia*
[5]*Graduate School of Engineering, Hokkaido University, Sapporo, Japan*
[6]*Geowissenschaftliches Zentrum Göttingen, Göttingen, Germany*

ABSTRACT

The Asachinskoe epithermal gold deposit in South Kamchatka, Russia, is a low-sulfidation type deposit which consists of Au-Ag bearing quartz-adularia-illite veins. Cathodoluminescence (CL) analysis using optical microscope and scanning electron microscope and trace element analysis of quartz using electron probe micro-analyzer (EPMA) were performed to elucidate the relationships between CL structures, trace element concentrations of different quartz generations, and metal precipitation mechanism of the Asachinskoe deposit. Five sequences of quartz crystallization can be distinguished within the mineralized vein of the bonanza zone. Most distinctive trace elements in quartz are Al (av. 1463 ppm) and K (av. 350 ppm). Colloform and microcrystalline quartz with moderate to dull red-brown CL coexists with electrum (Au-Ag alloy), naumannite-aguilarite (ss) and polybasite-pearceite (ss). The Au-Ag-Se precipitation is related to fluid boiling, and the Se enrichment is attributed to relative oxidizing mineralization conditions. Almost non-luminescent, dark brown luminescent quartz forming the matrix of the hydrothermal breccia coexists with electrum, tetrahedrite-tennantite (ss) and covellite. The Au-Ag-Cu precipitation is associated with rapidly precipitated quartz and adularia, and is due to sudden decompression and fluid boiling related to the hydrothermal brecciation.

Keywords: Cathodoluminescence, Trace Element, Quartz, Epithermal Gold deposit, Asachinskoe

INTRODUCTION

Cathodoluminescence (CL) designates the luminescence of UV to IR wavelengths induced by electron bombardment in minerals. CL can be caused either by intrinsic defects of the crystal lattice, such as non-stoichiometry (i.e., atomic vacancies) and structural imperfections (i.e., poor ordering, radiation damage, shock damage) or extrinsic defects related to luminescence-active impurities (i.e., trace elements) [1]. Variability in CL colors of quartz is a consequence of the heterogeneous incorporation and re-distribution of intrinsic defects and trace elements in the crystal structure during crystal growth and al-

*Corresponding author, e-mail: ryohei@nature.sci.hokudai.ac.jp
Information for use in citing this article: Okada, H., Mawatari, S.F., Suzuki, N. and Gautam, P. (eds.), *Origin and Evolution of Natural Diversity*, Proceedings of International Symposium "The Origin and Evolution of Natural Diversity", 1–5 October 2007, Sapporo, pp. 175–184.

teration [2–3]. Thus, CL analysis can reveal a wide range of growth and alteration textures that are useful for deciphering the formation history of multiple events that form mineralized veins and for distinguishing chronologic relationships between quartz precipitated at different times in a single vein [4].

Optical microscope (OM-) and scanning electron microscope (SEM-) CL and back scattered electron (BSE) images and the concentrations of Al, K, Ti, Fe and Mn using electron probe micro-analyzer (EPMA) in vein quartz were examined to elucidate the relationships between CL structures, trace element concentrations of different quartz generations, and metal precipitation mechanism of the bonanza zone of the Asachinskoe epithermal deposit. Distinguishing among the multiple generations of quartz precipitated in the Asachinskoe vein is critical for understanding the complex history of the multiple-stage vein formation.

GEOLOGIC OUTLINE

Geologic setting of study area

The Asachinskoe epithermal Au-Ag deposit is located in the southern part of the Porozhisto-Asachinskaya metallogenic province of South Kamchatka, Russia. The metallogenic province comprises volcanic and sedimentary rocks of Miocene age and plutonic rocks of Neogene age. Besides, Quaternary rocks associated with the Eastern Kamchatka volcanic belt are widely distributed ([5–6]; Fig. 1). The Eastern Kamchatka volcanic belt is splitted by the NW-oriented Nachikinskaya zone. Most of hydrothermal deposits and mineral occurrences are distributed along the Nachikinskaya zone, whereas the Asachinskoe deposit is isolated from them. The northwest of the deposit is overlain by Quaternary unit [5].

The Asachinskoe deposit is a low-sulfidation type of epithermal mineralization, which consists of forty N-oriented quartz-adularia-illite veins dominated by left-lateral shear and normal-faulting system over an area of 12 km^2. The mineralized veins are hosted by the Lower volcanic unit, Upper volcanic unit and subvolcanic dacite-andesite bodies. The Upper volcanic unit comprises coarse-grained dacite-andesite, tuff, tuff-breccia and lapilli-tuff. The Lower volcanic unit consists of volcaniclastic tuff. Both the Upper and Lower volcanic units are intruded by subvolcanic dacite and andesite bodies [7]. Propylitic alteration of the host rocks is widespread in the area, while argillic hydrothermal alteration, pyritization

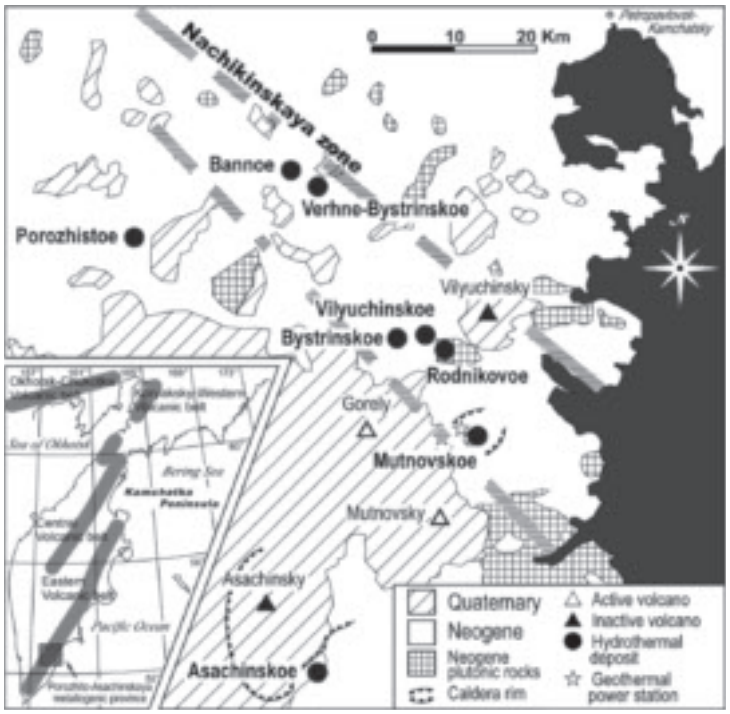

Fig. 1 Simplified geological map of the Porozhisto-Asachinskaya metallogenic province of South Kamchatka, Russia. Distribution of four volcanic belts is shown in the inset as gray thick lines–in NE Eurasia and Kamchatka Peninsula. Modified after Takahashi et al. (2007) [6].

and silicification with albite-sericite-smectite-pyrite-quartz is observed in the wall rock next to the mineralized vein [6]. On the basis of ore reserves estimation of ca. 20 t Au and 42 t Ag, an international joint-venture commenced exploitation of the deposit in 2005, and development of the Asacha mine in 2007, respectively [7].

Mineralization stages and their characteristics

The mineralized vein of the Asachinskoe deposit is divided into the Main Zone and Eastern Zone. A principal vein in the Main Zone, Vein No. 1, which branches into four veins above 200 masl (meters above sea level), is around 2 m in average thickness, reaching a maximum of 7 m. The bonanza level of Vein No. 1 is recognized around 200 masl, where four mineralization stages are distinguished based on macroscopic division criteria [6]. Stage I, a low grade Au mineralization, shows K-Ar age of 4.7 ± 0.2 Ma. Stage II is characterized by abundant illite, cryptomelane and Cu-bearing Mn-oxides and -hydroxides. Stage III (4.5–3.1 ± 0.1 Ma) forms a sulfide band with interfingering texture consisting of electrum (Ag/(Au + Ag) = 45–55 at.%), naumannite-aguilarite solid solution (ss) and polybasite-pearceite (ss). Stage IV is characterized by hydrothermal brecciation above 200 masl, where electrum with a wide compositional range (Ag/(Au + Ag)= 38–81 at.%), tetrahedrite-tennantite (ss) and covellite replacing tetrahedrite occur ([6]; Fig. 2). Concentrations of Au + Ag and $K_2O + Al_2O_3$ show a positive correlation, which indicates the association of gold and adularia precipitation. Stages III and IV are the most important gold mineralization stages. Fluid

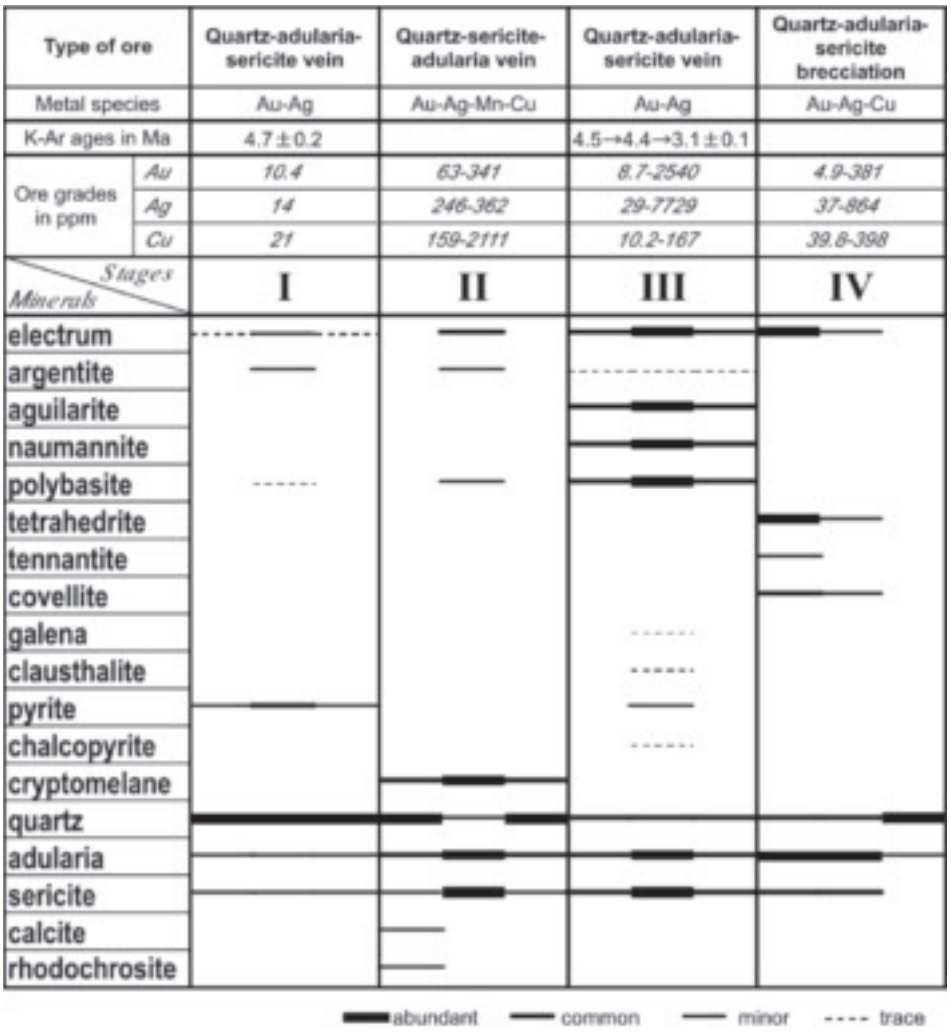

Fig. 2 Mineral paragenesis for the Main zone of the Asachinskoe deposit. Ore grades are based on bulk chemical compositions of hand specimens and their subdivided parts. After Takahashi et al. (2007) [6].

boiling (fluid inclusion data: ca. 160–190°C at 218 masl) and high Se content (> 100 ppm) are characteristic for Stage III, whereas fluid boiling, hydrothermal brecciation (170–180°C at 200 masl) and dusty and rhombic occurrence of adularia for Stage IV.

RESEARCH METHODOLOGY

Samples and preparation

Samples were collected from Vein No. 1 of the Main Zone at 200 masl (inside adit). Five Au-bearing quartz-adularia ores comprising Stages I, II, III and IV, and two host rocks which are cut by quartz-adularia veinlets, were prepared to be doubly polished thin sections coated with carbon.

Optical microscope cathodoluminescence

OM-CL color images were obtained using a hot-cathode luminescence microscope HC1-LM [8]. The electron gun operated at a voltage of 14 keV under high vacuum (10–5 mbar) and the applied filament current was 0.18 mA. The photographic documentation was carried out by a NIKON Microflex UFX-II system equipped with a NIKON FX-35A reflex camera. Color slides of luminescent quartz were taken with high-sensitive film KODAK Ektachrome 400 HC (400 ASA). The exposure times were of 100 to 250 sec using the 10x/0.30 objective.

Scanning electron microscope cathodoluminescence

SEM-CL images were obtained from the polished and carbon-coated thin sections using a LEO 1450 VP analytical SEM with an attached CENTAURUS BS BIALKALI type CL detector at the Geological Survey of Norway in Trondheim. The applied acceleration voltage and current at sample surface was 20 kV and~10 nA, respectively. The BIALKALI tube has a CL response range from 300 (violet) to 650 nm (red). It peaks in the violet spectrum range around 400 nm. The CL images were collected from one scan of 43 sec photo speed and a processing resolution of 1024 × 768 pixels and 256 gray levels. The brightness and contrast of the collected CL images were improved with the PhotoShop software.

Electron probe micro analysis

Trace element abundances of Al, K, Ti, Fe, and Mn in quartz were analyzed using a JEOL 8900 RL electron probe micro-analyzer (EPMA) at the Geowissenschaftliches Zentrum Göttingen, Germany. These elements are the most common trace elements in natural quartz beside H, Na and Li (e.g. [9]). K was selected as representative of the interstitial monovalent ions, because the detection limit of Na (~90 ppm) was higher than the typical concentrations and Li and H cannot be measured by EPMA. For high precision and sensitivity, a beam current of 80 nA, a beam diameter of 5 μm, and counting times of 15 sec for Si, and of 300 sec for Al, Ti, K, and Fe were used. Detection limits (3 sigma of single point background) were 12 ppm for Al, 10 ppm for K, 18 ppm for Ti, 24 ppm for Fe, and 24 ppm for Mn.

RESULTS

Characteristics of cathodoluminescence

The analysis based on 127 SEM-CL black-and-white images including 22 OM-CL color images revealed five sequences of quartz crystallization related to the macroscopic mineralization Stages I-IV. Representative SEM-CL images of quartz are shown in Fig. 3, where ore and gangue minerals are distinguished in BSE images.

Sequence 1 (Stage I): The oldest quartz crystallization stage caused intense silicification of the host rock and formed the primary quartz vein system. The quartz in the host rock shows microcrystalline texture with dull red-brown CL, however, no intragranular textures could be detected due to the small grain size. Subhedral quartz, which coexists with rhombic adularia or develops in open space, show moderate CL intensity with dull red-brown to yellow color (Fig. 3A). This subhedral quartz has 2–3 growth zones. Quartz of Sequence 1 is related to the formation of pyrite.

Sequence 2 (Stage II): Sequence 2 is characterized by crenulated layers (500 μm to several millimeters) of microcrystalline and equi-granular quartz with needle-like micro texture. The microcrystalline quartz generally has moderate CL intensities. However, red-brown CL at initial growth of the each layer and moderate to bright red CL at the final growth of the layers was observed. CL and BSE image analyses revealed co-genetic mineralization of adularia-illite, and electrum-quartz-adularia during final stage of this sequence.

Sequence 3 (Stage III): Sequence 3 is characterized by fine-crystalline quartz intergrown/co-genetic with euhedral adularia (50–500 μm). The quartz has moderate to dull red-brown CL, and the CL contrast reveals complex initial colloform and final euhedral growth zoning within crystals (Fig. 3C). Usually 5–

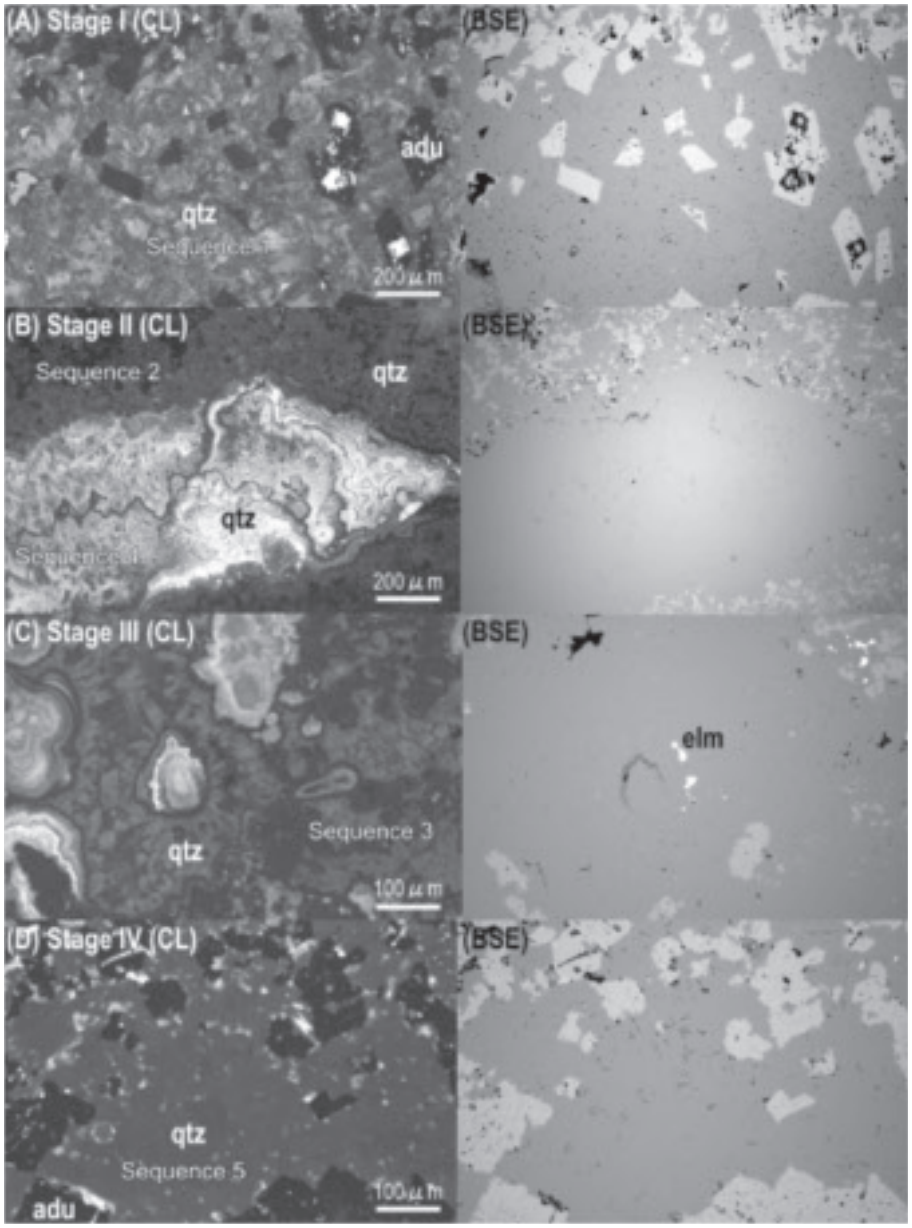

Fig. 3 Scanning electron microscope cathodoluminescence (SEM-CL) and backscattered secondary electron (BSE) images of quartz sequences 1–5 developed in the ores of Stages I-IV. SEM-CL images illustrate the complexity of quartz textures, and BSE images allow the rapid discrimination of quartz (qtz), adularia (adu) and electrum (elm).

15 growth zones can be identified, where zones with dark CL are microscopically associated with Au-Ag precipitation. Host rock structures were completely overprinted during this sequence.

Sequence 4 (Stage IV): Sequence 4 is characterized by bright yellow luminescent quartz, which fills open cavities in host rock and vein quartz of Stages I to III. Quartz shows oscillatory, sector zoning and occasionally colloform zoning with extremely high CL contrasts (Fig. 3B). The early quartz generation of this sequence is linked to Au-Ag precipitation.

Sequence 5 (Stage IV): Sequence 5 is characterized by non-luminescent or nearly non-luminescent quartz of equi-granular texture (25–50 μm; Fig. 3D). Color CL analysis revealed brown to dark brown CL, however growth zoning is not developed. This non-luminescent quartz impregnates former sequences and replaces their generations almost completely.

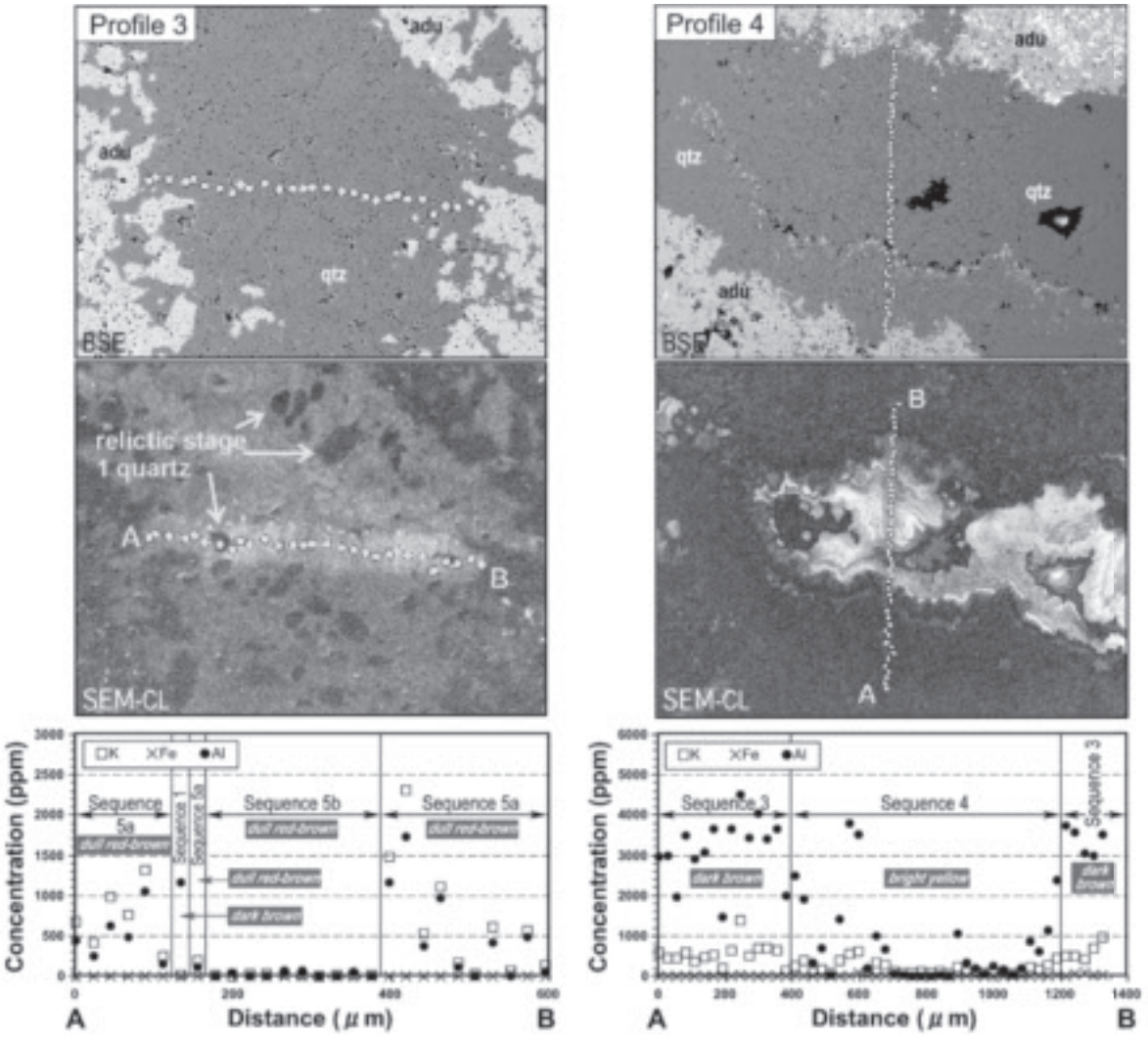

Fig. 4 Trace element concentrations measured by electron probe micro-analyzer. Profiles of step scanning are shown in BSE and SEM-CL images. Abbreviations are qtz for quartz and adu for adularia.

Trace element abundances in quartz

Trace element abundances were determined in 137 analytical points in total along 5 profiles, which passed across different quartz generations. Representative profiles (No. 3 and 4) are presented in Fig. 4. Ranges and averages of concentrations of Al, K, Ti, Fe, and Mn in quartz in Sequences 1–5 are given in Table 1. Al contents versus the Al/K and Al/Fe ratios are plotted in diagrams (Fig. 5).

The analyses reveal that Al and K are the most distinctive trace elements in quartz. Concentration of Ti is lower than the limit of detection of 18 ppm. Sequences 2 and 3 have very high average Al of 2920 and 2958 ppm and K of 556 and 452 ppm, respectively (Table 1). A pinkish-red luminescent quartz layer in Sequence 2 is highly enriched in Mn and Fe (av. 194 and 80 ppm, respectively). Sequences 4 and 5 are characterized by much lower Al but commonly high K contents (Fig. 5). Sequence 5 was subdivided into Sequences 5a and 5b based on compositional variation. Sequence 5a has high Al (av. 489 ppm) and very high K (av. 684 ppm), whereas the trace element concentrations of Sequence 5b are below the limit of detection (Fig. 4).

DISCUSSIONS

Cathodoluminescence and trace element signatures in mineralization sequences

SEM-CL analysis of quartz clarified that the host rocks were silicified primarily by Sequence 1 and overprinted by Sequences 3–4. Vein quartz of Se-

Table 1 Ranges and averages of trace element concentrations in quartz.

Stages	Quartz Sequences	Number of analysis	K (ppm) (d. l. = 10)	Ti (ppm) (d. l. = 18)	Fe (ppm) (d. l. = 24)	Al (ppm) (d. l. = 12)	Mn (ppm) (d. l. = 24)
I	**1**	1	17	< 18	< 24	1161	< 24
II	**2**	22	139–2736 (556)	< 18	< 24–239 (**80**)	1613–5081 (**2920**)	< 24–574 (**194**)
III	**3**	31	147–1394 (452)	≤ 18	≤ 32	1473–4495 (**2958**)	≤ 26
IV	**4**	55	23–1053 (167)	< 18	≤ 28	< 12–3777 (624)	< 24
IV	**5a**	18	25–2310 (**684**)	< 18	< 24	< 12–1729 (489)	≤ 31
IV	**5b**	10	< 10–26 (≤ 17)	< 18	< 24	< 12–71 (≤ 31)	< 24

Abbreviation: (d. l.) detection limit in ppm

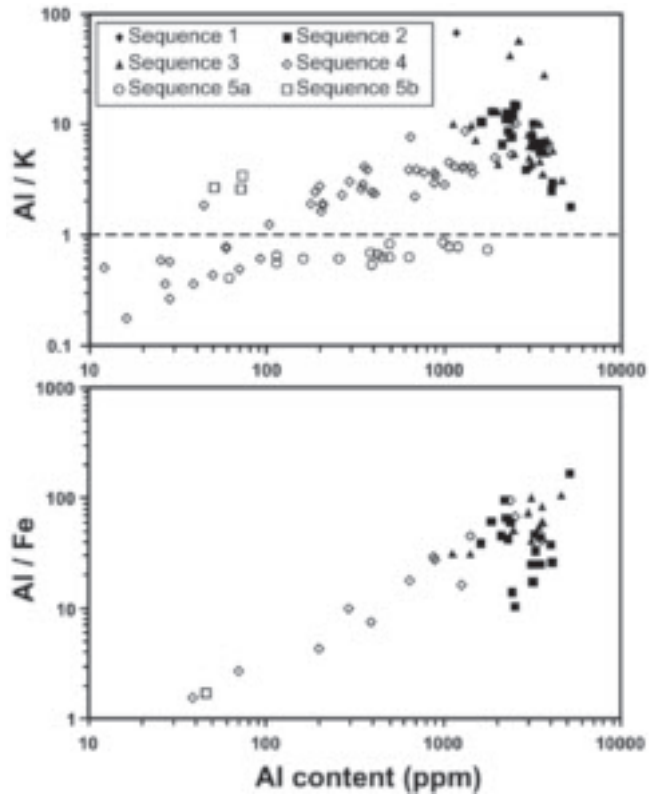

Fig. 5 Diagrams of K/Al and Al/Fe ratios versus Al content in quartz determined by electron probe micro-analyzer (EPMA).

quence 1 associated with the pyrite mineralization shows several growth zones (Fig. 3A). Layered microcrystalline quartz in Sequence 2 shows variable CL intensities with red-brown, bright red and pinkish red colors with high Mn (av. 194 ppm) and Fe (av. 80 ppm) contents, indicating that Mn-Fe enriched fluids entered the system. These Mn-Fe enriched fluids would be attributed to oxidation of formerly mineralized rhodochrosite and pyrite (Fig. 2). The SEM-CL and BSE observations indicate a rhythmic crystallization of quartz and adularia associated with electrum precipitation in Sequence 3. The colloform texture of some quartz in Sequence 3 originated from amorphous silica that precipitated under supersaturated conditions (e.g., [10]). Trace element analysis shows very high Al concentrations (av. 2909 ppm) and Al/K ratios (av. 10.8) of quartz in Sequences 1–3, which can be distinguished from Sequences 4–5 (av. 522 ppm, 2.5, respectively; Fig. 5). It is concluded that Sequences 1–3 (Stages I–III) crystallized in a static environment.

Layered colloform quartz in Sequence 4, which fills open cavities of a few millimeter scale, shows extremely high CL intensities with yellow color. Se-

quence 4 is observed in the host rock and Stages I-III. Colloform CL structures of Sequence 4 quartz indicate rapid precipitation of amorphous silica under supersaturated conditions at the initial stage of hydrothermal brecciation. Sequence 5 forms the main part of Stage IV that is characterized by intense hydrothermal brecciation. Quartz cementing the breccia structures is non-luminescent or nearly non-luminescent and appears black in the SEM-CL images. Previous studies on porphyry-style deposits have shown that quartz precipitated during hydrothermal breccia has very weak CL [11–13] and this may indicate that very low CL intensity is typically for quartz associated with precious metal precipitation. Our study distinguished K-Al enriched Sequence 5a and trace-element depleted Sequence 5b (Fig. 4). Sequence 5a is related to Au-Ag-Cu precipitation, and Sequence 5b is probably related to vein re-opening. It is concluded that quartz generations in Sequences 4–5 precipitated during hydrothermal brecciation.

Incorporation of trace elements in quartz

Quartz in Sequences 1, 2, 3, 4 and 5a has high Al (av. 1576 ppm) and K (av. 376 ppm). Both elements correlate positively. The high Al-K content is attributed to the high alkalinity of the hydrothermal solution that mineralized adularia [$KAlSi_3O_8$] and illite [$KAl_3Si_3O_{10}(OH)_2$]. The Al-K positive correlations are interpreted by the mechanism of substitutions of trivalent ions (i.e., Al^{3+} and Fe^{3+}) for Si^{4+} in SiO_2 structure and the incorporation of interstitial ions (i.e., K^+, Li^+, Na^+, H^+ and/or Fe^{2+}) as charge-compensators [e.g., 3].

Quartz in Sequence 5a shows very high K (av. 684 ppm) and high Al (av. 489 ppm) contents. Such high K contents have not been reported in literature before, in particular the fact that K is higher than Al. Quartz in Sequence 5a coexists with dusty and rhombic adularia. This dusty and rhombic adularia has a mineralogically unstable characteristics that are represented by the lower (= insufficient) mode compositions based on semi-quantitative XRD analysis compared to bulk chemical compositions than the data in Sequence III [6]. Rapid precipitation of quartz and abundant adularia might cause temporal Al depletion of the hydrothermal solution, and resulted in $Al/K < 1$ incorporation into quartz. Relatively low Al/Fe ratio (1.5–169) and a positive correlation between Al/Fe ratio and Al contents in Sequence 4–5 are result of increase of oxidized iron in the quartz-forming solution.

Au-Ag-Se Mineralization

BSE image analysis revealed microscopic sub-sequences of mineralization in Sequence 2 (Stage II), i.e., 1st) adularia-illite, and 2nd) electrum-quartz-adularia. Mn-oxide and hydroxide minerals and high Mn contents of quartz in Stage II would be related to oxidizing conditions. Development of colloform structures in quartz associated with electrum in Sequence 3 (Stage III) indicates supersaturation and rapid precipitation of amorphous silica. The supersaturation of silica would be due to vapor loss during the fluid boiling (ca. 160–190°C in Stage III). The interfingering texture of Au-Ag bearing sulfide band is interpreted as a replacement texture of platy calcite during Stage III. On the basis of these evidences and the previous studies [14–16], precipitation of electrum is interpreted by a mechanism of decomposition of Au thio complex due to CO_2 and H_2S degassing. Besides, selenium enriched composition in naumannite-aguilarite (ss) is due to a relatively oxidizing condition [17–18].

Au-Ag-Cu mineralization

Fluid boiling (170–180°C) in Stage IV (Sequence 5b) above 200 masl of Vein No. 1 would be a result of pressure release by hydrothermal brecciation. Sequence 5a shows a peculiar mineral paragenesis, i.e., electrum [Au-Ag], tetrahedrite-tennantite (ss) [$(Cu, Ag)_{10}(Fe, Zn)_2(Sb, As)_4S_{13}$] and secondary covellite [CuS] with quartz and dusty and rhombic adularia. In static hydrothermal environment of a low-sulfidation type gold deposit (e.g., $\log\Sigma S \fallingdotseq 2$, and neutral pH), usually electrum, argentite-naumannite (ss) [$Ag_2(S, Se)$], polybasite-pearceite (ss) [$(Ag, Cu)_{16}(As, Sb)_2(S, Se)_{11}$], chalcopyrite [$CuFeS_2$], pyrite [$FeS_2$] and sphalerite [ZnS] mineralize from the hydrothermal solution of dissolved (Au, Ag, Cu, Fe, Zn, Sb, As, S, Se) in the H_2O-H_2SiO_4-Al-Na-K-Ca-Mg-Cl-S-CO_2 system. Wide chemical composition ranges ($Ag/(Au + Ag) = 38–81$ at.%) of electrum is not buffered by the reaction $2Ag + 1/2S_2 = Ag_2S$ during Stage IV [19]. Above provided evidences, including very high K contents ($Al/K < 1$) in quartz, suggest that the mineralization was under non-equilibrium state. It is concluded that Au-Ag-Cu precipitation is associated with rapidly grown quartz and adularia, and due to sudden decompression and fluid boiling related to the hydrothermal brecciation.

CONCLUSIONS

SEM-CL analysis combined with trace element analysis revealed several quartz generations crystal-

lized in five sequences, overprinting history and chemical and redox conditions of hydrothermal fluid which have relationships with metal precipitation in the Asachinskoe deposit. Quartz of Sequences 1–3 (Stages I–III, respectively) crystallized under static conditions, whereas that of Sequences 4–5 (Stage IV) crystallized as a result of hydrothermal brecciation. The vein-side wall rock was affected by intense silicification during Sequence 1 and overprinted by Sequences 3 and 4. Quartz of Sequence 1 shows growth zoning, indicating a rhythmic crystallization. Quartz of Sequence 2 shows red-brown to bright red CL, and its trace element abundances indicate that Fe-Mn enriched fluid entered the system. Colloform and microcline quartz in Sequence 3 has moderate to dull red-brown CL indicating a supersaturation state. The Au-Ag-Se precipitation during Stage III (Sequence 3) would be due to fluid boiling, and Se enrichment could be attributed to relatively oxidizing conditions. Layered colloform quartz in Sequence 4 has bright yellow CL with complex growth zoning and precipitated at the initial stage of hydrothermal brecciation. Quartz in Sequence 5 is characterized to be dull red-brown CL. Quartz of sub-Sequence 5a has high K and Al, while quartz of sub-Sequence 5b is depleted in K, Ti, Fe, Al and Mn. The Au-Ag-Cu precipitation of Stage IV (Sequence 5a) is associated with rapidly grown quartz and adularia, and due to sudden decompression and fluid boiling related to the hydrothermal brecciation.

ACKNOWLEDGMENTS

This research was supported by the MEXT Grant-in-Aid for the 21st Century COE Program on "Neo-Science of Natural History" at Hokkaido University, Japan, and the Sasagawa Scientific Research Grant from The Japan Science Society. We would like to express our sincere gratitude to Vladimir I. Kudinov of SiGMA, Alexander Zalazaev and Anya U. Kim of ZAO Trevozhnoye Zaryevo, Jocelyn Waller and Marc Nally of Trans-Siberian Gold Plc., Anna M. Okrugina and Sergei Pozhkov of Institute of Volcanology and Seismology in Kamchatka, Yuuki Komata and Fumiaki Takeda of Hokkaido University, and Ksenia O. Shishcanova of Kamchatka State University for their helpful support during the field work and generous cooperation.

REFERENCES

1. Marshall, D.J., 1988. Cathodoluminescence of geological materials. Allen & Unwin Inc., Winchester/Mass., 146p.
2. Stevens Kalceff, M.A., Phillips, M.R., Moon, A.R. and Kalceff, W., 2000. Cathodoluminescence microcharacterization of silicon dioxide polymorphs. In: M. Pagel, V. Barbin, P. Blanc and D. Ohnenstetter (eds.), Cathodoluminescence in Geosciences, Springer, Berlin, 193–279.
3. Götze, J., Plötze, M. and Habermann, D., 2001. Origin, spectral characteristics and practical applications of the cathodoluminescence (CL) of quartz - a review. Mineral. Petrol., 71, 225–250.
4. Rusk, B.G. and Reed, M.H., 2002. Scanning electron microscope-cathodoluminescence of quartz reveals complex growth histories in veins from the Butte porphyry copper deposit, Montana. Geology, 30, 727–730.
5. Okrugin, V.M. and Zelensky, M.E., 2004. Miocene to Quaternary center volcanic, hydrothermal and ore-forming activity in the Southern Kamchatka. In: A.I. Khanchuk et al. (eds.), Metallogeny of the Pacific Northwest (Russian Far East): Tectonics, Magmatism and Metallogeny of Active Continental Margin, Interim IAGOD conf., excursion guidebook, 147–1769.
6. Takahashi, R., Matsueda, H., Okrugin, V.M. and Ono, S., 2007. Epithermal gold-silver mineralization of the Asachinskoe deposit in South Kamchatka, Russia. Resour. Geol., 57 (4), 354–373 (in press).
7. Trans-Siberian Gold PLC (TSG), 2004. Asacha Gold Project -Environmental Assessment. MDS Mining & Environmental Services LTD, UK, 137p.
8. Neuser, R.D., Bruhn, F., Götze, J., Habermannm, D. and Richter, D.K., 1995. Kathodolumineszenz: Methodik und Anwendung. Zentralbl. Geol. Paläontol., Teil 1, 1/2, 287–306.
9. Perny, B., Eberhardt, P., Ramseyer, K., Mullis, J. and Pankrath, R., 1992. Microdistribution of aluminium, lithium and sodium in a quartz: possible causes and correlation with shored lived cathodoluminescence. Am. Mineral., 77, 534–544.
10. Saunders, J.A., 1994. Silica and gold textures in bonanza ores of the Sleeper Deposit, Humboldt County, Nevada; evidence for colloids and implications for epithermal ore-forming processes. Econ. Geol., 894, 628–638.
11. Rusk, B. and Reed, M. 2002. Scanning electron microscope-cathodoluminescence analysis of quartz reveals complex growth histories in veins from the Butte porphyry copper deposit, Montana. Geology, 30, 727–730.
12. Müller A., Armstrong R., Herrington R., Seltmann R. 2003. Characterisation of quartz textures in porphyry copper ore deposits by scanning electron microscope-cathodoluminescence (SEM-CL). Mongolian Geoscientist, 21, 32–35.
13. Bayaraa, B., Bignall, G. and Tsuchiya, N., 2004. Geofluid dynamics of the Shuteen Mineralized Complex, Mongolia: results of a coupled SEM-CL and fluid inclusion study. In: abstr., 54th Congress of Resour. Geol., O-36, p. 60.
14. Seward, T.M., 1973. Thio complex of gold and the transfer of gold in hydrothermal ore solutions. Geochim. Cosmochim. Acta, 53, 379–399.
15. Seward, T.M., 1989. The hydrothermal chemistry of gold and its implications for ore formation: Boiling and conductive cooling as examples. Econ. Geol. Monogr., 6, 398–404.
16. Ohmoto, H. and Goldhaber, M.B., 1997. Sulfur and carbon isotopes. In: H.L. Barnes (ed.), Geochemistry of hydrothermal deposit. John Wiley & Sons, Inc., New York, 517–611.
17. Simon, G., Kesler, S.E. and Essene, E.J., 1997. Phase relations among selenides, tellurides, and oxides; II, Applications to selenide-bearing ore deposits. Econ. Geol., 92, 4, 468–

484.
18. Liu, J., Zheng, M., Liu, J. and Su, W., 2000. Geochemistry of the La'erma and Qiongmo Au-Se deposits in the western Qinling Mountains, China. Ore Geol. Rev., 17, 1, 91–111.
19. Barton, P.B., Jr. and Toulmin, P., III., 1964. The electrum-tarnish method for the determination of the fugacity of sulfur in laboratory sulfide system. Geochem. Cosmochem. Acta, 28, 619–640.